

# DAMM: Directionality-Aware Mixture Model Parallel Sampling for Efficient Dynamical System Learning

Sunan Sun,<sup>1</sup> Haihui Gao<sup>1</sup>, Tianyu Li<sup>1</sup> and Nadia Figueroa<sup>1</sup>

<sup>1</sup>Department of Mechanical Engineering, University of Pennsylvania, Philadelphia, PA 19104, USA

**Abstract:** The Linear Parameter Varying Dynamical System (LPV-DS) is a promising framework for learning stable time-invariant motion policies in robot control. By employing statistical modeling and semi-definite optimization, LPV-DS encodes complex motions via non-linear DS, ensuring the robustness and stability of the system. However, the current LPV-DS scheme faces challenges in accurately interpreting trajectory data while maintaining model efficiency and computational efficiency. To address these limitations, we propose the Directionality-aware Mixture Model (DAMM), a new statistical model that leverages Riemannian metric on  $d$ -dimensional sphere  $\mathbb{S}^d$ , and efficiently incorporates non-Euclidean directional information with position. Additionally, we introduce a hybrid Markov chain Monte Carlo method that combines the Gibbs Sampling and the Split/Merge Proposal, facilitating parallel computation and enabling faster inference for near real-time learning performance. Through extensive empirical validation, we demonstrate that the improved LPV-DS framework with DAMM is capable of producing physically-meaningful representations of the trajectory data and improved performance of the generated DS while showcasing significantly enhanced learning speed compared to its previous iterations.

## 1. Introduction

The safe integration of robots into human workspaces requires the ability to adapt and replan in response to changing environments and constraints. Traditional path planning approaches, assuming a known environment and robot dynamics, face challenges when confronted with uncertainties and perturbations during operation [1, 2, 3]. In contrast, Dynamical System (DS)-based motion policies leverage redundancy of solutions in dynamic environments, embedding a set of feasible solutions in a single control law to overcome environmental uncertainties [4]. Furthermore, stability conditions can be introduced as constraints in the learning of DS, providing a closed-form analytical solution to trajectory planning, with theoretical guarantees such as stability and convergence [5, 6].

In this paper, we consider the problem of learning a generalized motion policy from multiple demonstrations when the motion is time-independent. Recognizing nonlinear DS can be formulated as a mixture of linear time-invariant (LTI) systems, we consider the Linear Parameter Varying Dynamical System (LPV-DS) framework [6, 7, 8], which provides a comprehensive pipeline for learning time-invariant non-linear DS while exhibiting robustness to both spatial and temporal perturbations.

### 1.1. LPV-DS Formulation [6, 7, 8]

Let  $\xi \in \mathbb{R}^d$  and  $\dot{\xi} \in \mathbb{R}^d$  represent the kinematic robot state and velocity vectors; e.g., Cartesian coordinates/velocities of a robot arm's end effector, the position/velocity of a mobile robot, etc. In the DS-based motion policy literature [8],  $\dot{\xi} = f(\xi)$  is a first-order DS that describes a motion policy in the robot's state space  $\mathbb{R}^d$ . The goal of DS-based learning from demonstration (LfD) [6, 7, 8] is to infer  $f(\xi) : \mathbb{R}^d \rightarrow \mathbb{R}^d$  from data, such that any point  $\xi$  in the state space leads to a stable attractor  $\xi^*$ , with  $f(\xi)$  described by a set of parameters  $\Theta$  and attractor  $\xi^* \in \mathbb{R}^d$ ; mathematically  $\dot{\xi} = f(\xi; \Theta, \xi^*) \Rightarrow \lim_{t \rightarrow \infty} \|\xi - \xi^*\| = 0$ , i.e., the DS is globally asymptotically stable [9].

Learning the mapping function  $f(\xi)$  can be framed as a regression problem, where the inputs are the state variables  $\xi$  and the outputs are the first-order time derivative  $\dot{\xi}$ . Such formulation gives rise to the utilization of statistical methods for estimating the parameters  $\Theta$ . However, standard regression techniques cannot ensure global asymptotic stability. To alleviate this the LPV-DS approach was first introduced in the seminal work of [6] as a constrained Gaussian Mixture Regression (GMR) and then formalized as the untied Gaussian Mixture Model (GMM)-based LPV-DS approach in [7], where a nonlinear DS is encoded as a mixture of continuous LTI systems:

$$\dot{\xi} = f(\xi; \Theta) = \sum_{k=1}^K \gamma_k(\xi) (A_k \xi + b_k) \quad \text{s.t.} \quad \begin{cases} (A_k)^T P + P A_k = Q^k, Q_k = (Q_k)^T \prec 0 \\ b_k = -A_k \xi^* \end{cases} \quad (1)$$

where  $\gamma_k(x)$  is the state-dependent mixing function that quantifies the weight of each LTI system  $(A_k \xi + b_k)$  and  $\Theta = \{\theta_\gamma\}_{\gamma=1}^K = \{\gamma_k, A_k, b_k\}_{k=1}^K$  is the set of parameters to learn. The constraints on the right side of the Eq. 1 enforce global asymptotic stability of the resulting DS derived from a parametrized Lyapunov function  $V(\xi) = (\xi - \xi^*)^T P (\xi - \xi^*)$ . These constraints have been derived and proven in [6, 7, 8], yet for completeness we include the proof in Appendix A.

Interestingly, in order to ensure global asymptotic stability of Eq. 1, besides enforcing the Lyapunov stability constraints on the LTI parameters one must ensure that  $0 < \gamma_k(x) < 1$  and  $\sum_{k=1}^K \gamma_k(x) = 1 \quad \forall \xi \in \mathbb{R}^d$ . As noted in [7], this can be readily achieved by formulating the mixing function using the a posteriori probability of the state  $\xi$  from a GMM used to partition the nonlinear DS into linear components, where  $K$  is the number of components corresponding to the number of LTIs:

$$\gamma_k(\xi) = \frac{\pi_k \mathcal{N}(\xi | \theta_k)}{\sum_{j=1}^K \pi_j \mathcal{N}(\xi | \theta_j)} \quad \text{from} \quad p(\xi | \{\pi_k, \theta_k\}) = \sum_{k=1}^K \pi_k \mathcal{N}(\xi | \mu_k, \Sigma_k). \quad (2)$$

$\mathcal{N}(\xi | \theta_k)$  is the probability of observation  $\xi$  from the  $k$ -th Gaussian component parametrized by mean and Covariance matrix  $\theta_k = \{\mu_k, \Sigma_k\}$  and the prior probability of an observation from this particular component  $\pi_k$  satisfying  $\sum_{k=1}^K \pi_k = 1$ .

**$\Theta$  estimation:** In [7] a two-step estimation framework was proposed to estimate the GMM parameters  $\Theta_\gamma = \{\pi_k, \mu_k, \Sigma_k\}_{k=1}^K$  and the DS parameters  $\Theta_{DS} = \{A_k, b_k\}_{k=1}^K$  which combined results in the final set of parameters  $\Theta$ . First, given the set of reference trajectories  $\{\xi_i^{ref}, \dot{\xi}_i^{ref}\}_{i=1 \dots N}$ , where  $i$  is the sequence order of the sampled states, a GMM is fit to the position variables of the reference trajectory,  $\{\xi_i^{ref}\}_{i=1 \dots N}$ , to obtain  $\Theta_\gamma$ . The optimal number of Gaussians  $K$  and their placement can be estimated by model selection via Expectation-Maximization or via Bayesian non-parametric estimation. Then, the rest of parameters  $\Theta_{DS}$  in Eq. 1 are learned through a constrained optimization by introducing stability conditions and minimizing the difference between the estimated output  $\dot{\xi} = f(\xi)$  and the desired output  $\dot{\xi}^{ref}$ , as proposed in [7] and described in Appendix B.

## 1.2. Motivation

Given a reference trajectory, one can interpret that each subsystem in Eq. 1 locally governs a portion of the trajectory. Recall that the learning of each governing subsystem derives from its corresponding Gaussian component, it is natural to assume that the statistical model places each Gaussian on the near-linear segment. Such placement of Gaussians makes intuitive sense because Gaussian can be easily shaped in a long or slim manner to model linear trajectory. However, this is not always the case for standard GMM estimation techniques. As shown in the left column of Fig. 1, we show an example of the GMM fit to the position  $\xi$  only via standard Gibbs sampling, referred to as vanilla GMM. The clustering result fails to encapsulate the intrinsic motion of the original trajectory due to the lack of directionality, leading to an erroneous DS. Though one might be attempted to fit a GMM to the position and velocity  $\xi, \dot{\xi}$  together, we note that GMM adopts Euclidean distance measure while velocities are clearly non-Euclidean. As shown in the second left column of Fig. 1, the clustering result is not physically-meaningful, and such an inaccurate representation fails to encode the original trajectory, let alone produce a reliable DS.

**PC-GMM [7]:** To alleviate these issues, the Physically-Consistent GMM (PC-GMM) was proposed by Figueroa and Billard [7]; a state-of-the-art statistical model tailored to the LPV-DS framework. By applying a distance-dependent Chinese Restaurant Process (DD-CRP) prior [10], PC-GMM integrates a distance measure of direction by computing the pair-wise cosine similarity between every observation. Considering the directionality of the trajectories as side-information, PC-GMM captures the linear portions along the trajectory and produces more informative clustering results and DS, as shown in the second right column of Fig. 1. However, PC-GMM suffers from slow inference rate due to the formulation of the DD-CRP requiring the computation of an  $N \times N$  similarity matrix resulting in memory inefficiency and exponential increase in computation time wrt. number of datapoints in the reference trajectories  $N$ . Moreover, the online learning of PC-GMM is hard to achieve because the inference with the DD-CRP prior necessitates incremental updates [10], ruling out the possibility of parallel computation as such updates are *strictly sequential*. In addition, PC-GMM can produce inconsistent and inefficient clustering results, occasionally leading to excessive  $K$  Gaussians for simple reference trajectories. This is attributed to the lack of a regulation mechanism to control the desired number of components  $K$ .



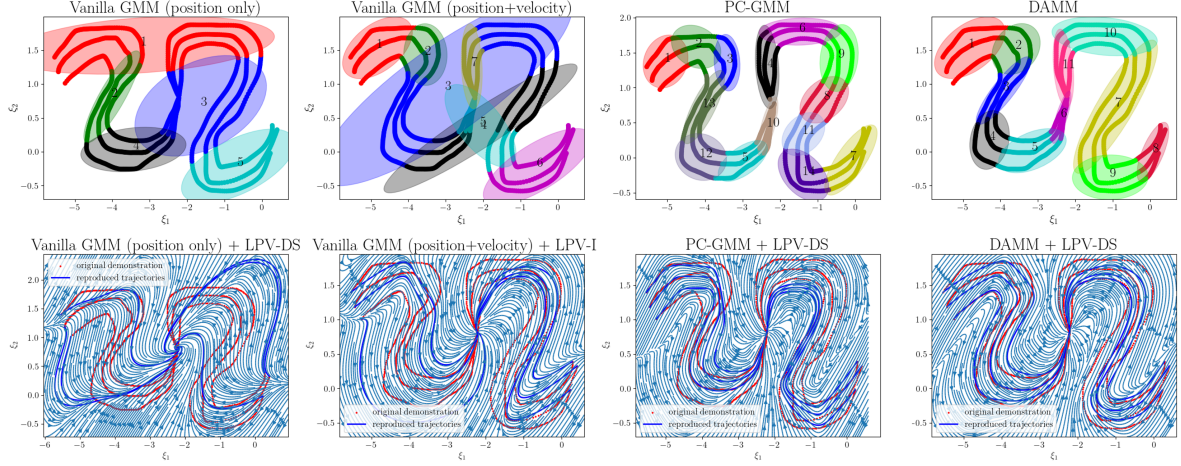


Fig. 1: Comparison between the Vanilla-GMM (position only) LPV-DS, Vanilla-GMM (position+velocity) LPV-DS, PC-GMM LPV-DS and **DAMM LPV-DS** on a multi-behavior trajectory. Vanilla-GMM refers to GMM fitted via Gibbs Sampling. Top row shows the clustering results; bottom row shows the LPV-DS results. Datasets obtained from [7]. The computation time are 5, 8, 55 and 0.8 in seconds from left to right, and the number of components are 5, 7, 14 and 11. Notice the improved reproduction accuracy resulting from optimal GMM fitting via DAMM on the right column.

### 1.3. Our approach & Contributions

In tackling the aforementioned challenges of PC-GMM, we introduce the Directionality-Aware Mixture Model (DAMM). Inspired by prior work on clustering spherical data on Riemannian manifolds [11], the DAMM formulation augments the state variables  $\xi \in \mathbb{R}^d$  with directional information of the trajectories using a proper Riemannian metric on the directional data manifold, inherently capturing the directional information or the trend of motion along the reference trajectories. We then introduce a generative model and a new parallel Markov chain Monte Carlo (MCMC) sampling scheme to find the optimal  $K$  that can achieve online performance tailored to the DAMM formulation. These innovations offer computationally efficiency, model efficiency and directional consistency for online estimation of LPV-DS motion policies from demonstrations in  $< 500ms$ . As shown on the right columns of Fig. 1, the DAMM-based LPV-DS successfully senses the directionality and identifies the linear portions of trajectories, resulting in physically-meaningful DS shown on the bottom right with less number of Gaussian  $K$  than PC-GMM and with an unprecedented estimation time.

We evaluate our approach through extensive empirical validation, including benchmark comparisons on LASA datasets [12] and the PC-GMM dataset [7] (including 2D and 3D real trajectories) against PC-GMM and baseline sampling approaches, as well as real robot experiments. We demonstrate that the DAMM-based LPV-DS framework exhibits enhanced capabilities in producing improved DS across various metrics, and achieves an order of magnitude faster rate of learning speed compared to its predecessor, allowing for efficient and nearly online learning performance. To the best of our knowledge, this is the first DS learning framework that can be estimated in such near real-time scale.

## 2. Directionality-Aware Mixture Model Parallel Sampling

### 2.1. Directionality-Aware Mixture Model (DAMM)

Consider the LPV-DS formulation introduced in Sec. 1.1, the demonstration trajectory consists of position  $\xi$  and velocity  $\dot{\xi}$  at each observation. As demonstrated in Section 1.2 and further in Appendix H concatenating  $\xi$  and  $\dot{\xi}$  to fit the GMM is an ill-posed strategy as Euclidean distances on directional data cannot properly represent similarity in directional vectors.

We begin the formulation of the DAMM by normalizing the velocity and obtain the unit-length directional vector for each observation,  $\xi^{dir} = \frac{\dot{\xi}}{\|\dot{\xi}\|} \in \mathbb{S}^{d-1} \subset \mathbb{R}^d$ , lying on the  $(d-1)$ -dimensional unit sphere and capturing the trend of motion in a trajectory. Since the unit sphere is a nonlinear Riemannian manifold with positive definite inner product defined on the tangent space, one can define the Riemannian equivalent of mean and covariance for directional data:

$$\mu^{dir} = \underset{p \in \mathbb{S}^{d-1}}{\operatorname{argmin}} \sum_{i=1}^N d(\xi_i^{dir}, p)^2 \quad \& \quad \Sigma^{dir} = \frac{1}{N} \sum_{i=1}^N \log_{\mu^{dir}}(\xi_i^{dir}) \log_{\mu^{dir}}(\xi_i^{dir})^T \quad (3)$$

where the directional mean  $\mu^{dir} \in \mathbb{S}^{d-1}$  is defined as the center of mass on the unit sphere, and  $d(\cdot, \cdot)$  is the geodesic distance between two points [13, 14]. We provide the  $\exp/\log$  and  $d(\cdot)$  equations for the unit sphere manifold in Appendix C. Analogous to the shortest distance being the straight line between two points in Euclidean space, the geodesic defines the Riemannian equivalent of distance. Directional mean  $\mu^{dir}$  employs the notion of the Fréchet mean [15], which extends the sample mean from  $\mathbb{R}^d$  to Riemannian manifolds  $\mathcal{M}$ . In practice,  $\mu^{dir}$  can be efficiently computed in an iterative approach [16]. The empirical covariance  $\Sigma^{dir}$  captures the dispersion of directional data in the tangent space  $T_p \mathbb{S}^{d-1}$ , where the logarithmic map  $\log_x : \mathcal{M} \rightarrow T_x \mathbb{S}$  maps a point on the Riemannian manifold to the tangent space defined by the point of tangency  $x$ . The inverse map is the exponential map  $\exp_x : T_x \mathbb{S} \rightarrow \mathcal{M}$  which maps a point in the tangent space of  $x$  to the manifold so that the mapped point lies in the direction of the geodesic starting at  $x$  [16, 17, 18].

Although both  $\mu^{dir}$  and  $\Sigma^{dir}$  are well defined in Riemannian geometry and have been widely used in Riemannian statistics, we are not interested in the covariance  $\Sigma^{dir}$  that *fully* captures the variation with respect to different directions in the manifold's geometry. Recall the goal of DAMM is not to cluster velocity, but to recognize the linear segment in a nonlinear trajectory and retrieve the corresponding Gaussians. Hence, only the variation of direction within a linear component needs to be accounted for, and we define such variation as follows:

$$(\sigma^2)^{dir} = \frac{1}{N} \sum_{i=1}^N d(\xi_i^{dir}, \mu^{dir})^2 = \frac{1}{N} \sum_{i=1}^N \|\log_{\mu^{dir}}(\xi_i^{dir})\|_2^2 \quad (4)$$

where the variance  $(\sigma^2)^{dir}$  is a scalar value describing the variation in the magnitude of direction with respect to mean. We note again that though the variance is reduced from its full dimension to a scalar value, this is desired because the new model would only care about the variation in direction within a linear component. In other words, if a cluster contains a large variance  $(\sigma^2)^{dir}$ , then it is considered non-linear and should be split in a way that the new clusters retain lower variances  $(\sigma^2)^{dir}$ , resembling linear components. Eq. 4 follows that fact the geodesic is equal to the  $l_2$  norm of one point being mapped onto the tangent space via the logarithmic map defined by the point of tangency [13, 14].

Now we define the the new state variable and the respective *statistic* for the DAMM:

$$\hat{\xi} = \left( \begin{array}{c} \xi^{pos} \\ \|\log_{\mu^{dir}}(\xi^{dir})\|_2 \end{array} \right) \quad \& \quad \hat{\mu} = \left( \begin{array}{c} \mu^{pos} \\ 0 \end{array} \right) \quad \& \quad \hat{\Sigma} = \left( \begin{array}{cc} \Sigma^{pos} & 0 \\ 0 & (\sigma^2)^{dir} \end{array} \right). \quad (5)$$

The new state  $\hat{\xi}$  is augmented with the geodesic between its own direction and the directional mean, which is not a unique value and varies with respect to different directional mean  $\mu^{dir}$ . The new mean  $\hat{\mu}$  is augmented with a zero because the geodesic of mean is always zero with respect to itself. The variance  $(\sigma^2)^{dir}$  is attached along the diagonal in the new covariance  $\hat{\Sigma}$  where all the off-diagonal entries are zero except the ones in  $\Sigma^{pos}$ . The correlation is removed intentionally because again the DAMM only accounts for the variation in direction within a Gaussian, and should avoid any intertwining between position and direction.

## 2.2. DAMM Generative Model

We now define the generative model for the DAMM:

$$\begin{aligned} \pi &\sim GEM(1, \alpha) \\ z_i &\sim Cat(\pi_1, \pi_2, \dots) \\ \hat{\xi}_i | z_i = k &\sim \mathcal{N}(\hat{\mu}_k, \hat{\Sigma}_k) \end{aligned} \quad (6) \quad p(\hat{\xi} | \theta_\gamma) = \sum_{k=1}^K p(z_i = k) \mathcal{N}(\hat{\xi} | \hat{\mu}_k, \hat{\Sigma}_k) \quad (7)$$

The generative DAMM first samples the infinite-length cluster proportions,  $\pi$  from a GEM (Griffiths Engen McCloskey) distribution following the stick-breaking process [19]. The cluster assignment of each data point  $z_i$  is sampled from the categorical distribution defined by  $\pi$ . An observation  $\hat{\xi}_i$  is then drawn from its associated Gaussian whose parameters follow the same form as in Eq. 5. Given the generative model, the density function of DAMM is defined by Eq. 7, where  $\theta_k = \{\hat{\mu}_k, \hat{\Sigma}_k\}_{k=1}^K$  is the set of parameters defining each Gaussian component.

Note that the drawing of the parameters  $\{\hat{\mu}_k, \hat{\Sigma}_k\}$  is sampled from the the Normal-Inverse-Wishart (*NIW*) distribution, which is the conjugate prior of a multivariate Normal distribution [20]:

$$(\hat{\mu}, \hat{\Sigma}) \sim NIW(\Psi, \nu, \mu_0, \kappa) \quad \equiv \quad \hat{\Sigma} \sim IW(\Psi, \nu); \quad \hat{\mu} | \hat{\Sigma} \sim \mathcal{N}(\mu_0, \hat{\Sigma}/\kappa) \quad (8)$$

where the covariance  $\hat{\Sigma}$  is drawn from an Inverse Wishart distribution, and the mean is drawn from a normal distribution conditioned on the covariance. We note that the hyperparameters  $\Psi, \mathbf{v}$  embody the prior belief on the covariance, and therefore we have the control over the variation in direction. In other words, we can treat these hyperparameters as a regulation mechanism to decide how much  $(\sigma^2)^{dir}$  in Eq. 4 is allowed within each component. For example, given a nonlinear trajectory, if the prior belief is that  $(\sigma^2)^{dir}$  is high, then a larger variation in direction is tolerated and DAMM will produce fewer components. And vice versa, meaning more components will be produced to respect the prior belief about a low variance  $(\sigma^2)^{dir}$ .

### 2.3. Parallel Sampling

DAMM achieves parallel sampling by employing an efficient sampling method by mixing the Gibbs sampler and the Split/Merge Proposals. Note that Gibbs samplers fall under two categories: collapsed-weight (CW) Gibbs sampler and instantiated-weight (IW) Gibbs sampler [21]. CW Gibbs sampler used in PC-GMM would marginalize out the parameters and require incremental update of each data point [7, 10]. On the other hand, IW sampler would instantiate all the parameters in the beginning of every iteration and sample all data points at once. The downside of IW Gibbs sampler is that it can only instantiate a finite number of parameters, which is not the case for the infinite-length cluster proportions in the DAMM model, and it cannot create new clusters. However, Chang and Fisher III [22] proves that if IW Gibbs sampler is mixed with any split mechanism that produces new component, then the result chain is indeed ergodic and the mixed sampler is a valid MCMC method. Hence, we introduce the new efficient sampler that combines IW Gibbs sampler and Split/Merge Proposal that caters to the inference of the DAMM model.

#### 2.3.1. Instantiated Gibbs Sampler

Given the generative model of the DAMM in Eq. 7, and the conjugate prior defined in Eq. 8, each variable can be sampled from the posterior distribution via an IW Gibbs sampler as follows [20],

$$\begin{aligned} (\pi_1, \dots, \pi_K, \tilde{\pi}_{K+1}) &\sim \text{Cat}(N_1, \dots, N_K, \alpha), \\ (\hat{\mu}_k, \hat{\Sigma}_k) &\sim \mathcal{N}(\xi_{\{k\}} | \hat{\mu}_k, \hat{\Sigma}_k) NIW(\Psi, \mathbf{v}, \mu_0, \kappa) = NIW(\Psi_n, \mathbf{v}_n, \mu_n, \kappa_n), \quad \forall k \in \{1, \dots, K\} \\ z_i &\sim \sum_{k=1}^K \pi_k \mathcal{N}(\hat{\xi}_i | \hat{\mu}_k, \hat{\Sigma}_k), \quad \forall i \in \{1, \dots, N\}. \end{aligned} \quad (9)$$

Say the system has  $K$  number of components in the beginning of an iteration, the realization of each variable can only come from one of  $K$  options. We first draw the cluster proportions  $\pi$  from a categorical distribution defined by the number of observations  $N_k$  associated with  $k_{th}$  component and the concentration factor  $\alpha$ , then draw the parameters of each component from a  $NIW$  distribution parametrized by  $(\Psi_n, \mathbf{v}_n, \mu_n, \kappa_n)$ , and lastly draw the assignment of each observation proportional to the density function multiplied by the proportion  $\pi$  for each component. We note that, as mentioned before, each procedure in Eq. 9 can be parallelized, but cannot create new components. Hence, the result Markov chain is non-ergodic; i.e. not every states can be visited and no guarantees of convergence.

#### 2.3.2. Split/Merge Proposals

Split/Merge proposal was first introduced as an alternative MCMC method to CW Gibbs sampler for escaping low-probability local modes [23]. Unlike the incremental nature of CW Gibbs sampler by moving one data point at a time within iteration, Split/Merge proposal moves a group of data points at once. The original formulation of the Split/Merge Proposal, however, still employs the partial use of CW Gibbs sampler to produce appropriate proposals, hindering parallel computation. We therefore introduce the modified Split/Merge Proposal tailored to the aforementioned IW Gibbs sampler.

In the context of a Hidden Markov Model, we treat the assignment of each observation as latent variables and employ MCMC methods to draw a sample from the posterior distribution after seeing observations. Hence, we designate  $z \in \mathbb{R}^N$  as the hidden state of the model which is a long vector containing the assignments of  $N$  observations, and  $\xi$  as the observations. Say we are at a particular state  $z$  in Markov chain, we can propose a candidate state either by a split or a merge  $z^*$  and then decide if the candidate proposal is accepted or not by evaluating the Metropolis-Hasting acceptance probability as follows [24, 25],

$$a(z^*, z) = \min \left[ 1, \frac{q(z|z^*) \pi(z^*)}{q(z^*|z) \pi(z)} \right] = \min \left[ 1, \frac{p(z|z^*) p(z^*|\xi)}{p(z^*|z) p(z|\xi)} \right] \quad (10)$$

where the target distribution  $\pi(z)$  is the posterior distribution  $p(z|\xi)$  we draw sample from, and the proposal distribution  $q(z^*|z)$  is the probability of reaching the candidate state  $z^*$  from the current state  $z$ , i.e.,  $p(z^*|z)$ . We now look at each term in the context of **split** as an example. As advised in [23], random split or merge is highly unlikely to be accepted. Hence, we define a launch state  $z^{launch}$  and treat it as a pseudo current state in place of the original  $z$  in Eq. 10. We reach the launch state by performing multiple scans of IW Gibbs only within the component we propose to split; i.e., we leave other observations unchanged and only re-assign the labels of the affected observations assuming a split occurs. If conjugacy is satisfied [20], the ratio of target distribution has the following analytical forms:

$$\frac{p(z^{split}|\xi)}{p(z|\xi)} = \frac{\prod_{z_i=z_1^{split}} \pi_1 \mathcal{N}(\xi_{z_i}|\mu, \Sigma)_{\{z_1^{split}\}} \prod_{z_i=z_2^{split}} \pi_2 \mathcal{N}(\xi_{z_i}|\mu, \Sigma)_{\{z_2^{split}\}}}{\prod_{z_i=z_{12}^{split}} \mathcal{N}(\xi_{z_i}|\mu, \Sigma)_{\{z_{12}^{split}\}}} \quad (11)$$

where  $\{z_i = z_1^{split}\}$  is the set of observations assigned to the first split group,  $\{z_{12}^{split}\}$  is the group proposed to be split,  $(\pi_1, \pi_2)$  are the cluster proportions and  $\mathcal{N}(\cdot)_{\{z_k\}}$  is the probability density of Normal distribution defined by the set of observations assigned to  $z_k$ . Notice how the unchanged assignments are cancelled out and only the affected ones stay in Eq. 11.

The ratio of proposal distribution in Eq. 10 describes the probability of reaching the candidate state from the launch state by *one* scan of IW Gibbs sampler. Given the IW Gibbs sampler in Eq. 9, we derive the following form:

$$\frac{P(z|z^{split})}{P(z^{split}|z)} = \prod_{z_i=z_1^{launch}} \prod_{z_i=z_2^{launch}} \frac{\pi_{z_1^{launch}} \mathcal{N}(\xi_{z_i}|\mu, \Sigma)_{\{z_1^{launch}\}} + \pi_{z_2^{launch}} \mathcal{N}(\xi_{z_i}|\mu, \Sigma)_{\{z_2^{launch}\}}}{\pi_{z_i} \mathcal{N}(\xi_{z_i}|\mu, \Sigma)_{\{z_i\}}} \quad (12)$$

Now we can substitute the Expressions 11 and 12 into the acceptance ratio in Eq. 10 and evaluate if the candidate state is accepted or not. By cycling between split and merge proposal, the result Markov chain is ergodic. The **merge** proposal formulation is detailed in Appendix D.

## 2.4. Mixed Sampler

We have shown that Split/Merge proposal is capable of producing new components, making it a well-suited complement to the IW Gibbs sampler for constructing an ergodic Markov chain. The combined sampler effectively alternates between the two MCMC methods in the following manner:

1. IW Gibbs sampler rearranges the entire assignments across the current number of components for multiple scans by Eq. 9.
2. Then split is proposed and evaluated for each existing components by Eq. 10, followed by additional scans by the IW Gibbs sampler across the new assignments by Eq. 9.
3. Finally multiple merge proposals are evaluated by Eq. 10.
4. Repeat step 1-3 until convergence.

To propose meaningful merge between appropriate groups, instead of choosing randomly, we pick two candidates using metrics such as Gaussian similarity and Euclidean distance between means. The number of iterations within each step remains a heuristic that must be set empirically.

## 3. Experimental Results

### 3.1. Evaluation and Comparison

We conduct a comprehensive benchmark evaluation of the DAMM-based LPV-DS framework on the LASA handwritten dataset [6, 7] and compare its performance to the baseline the PC-GMM-based LPV-DS. The LASA handwritten dataset consists of 30 motion sets, each containing 7 trajectories. We perform an evaluation of our approach on the entire LASA dataset, using 6 different metrics.

The metrics on statistical models are (i) computation time (ii) Bayesian information criterion (BIC) (iii) Akaike information criterion (AIC). Both BIC and AIC take into account the likelihood of the data given the model and the number of model parameters, providing a good measurement of model complexity. The metrics on DS are:

- (i) prediction RMSE =  $\frac{1}{N} \sum_{i=1}^N \|\dot{\xi}_i^{ref} - f(\xi_i^{ref})\|$  (ii) prediction cosine similarity,  $\dot{e} = \frac{1}{N} \sum_{i=1}^N |1 - \frac{f(\xi_i^{ref})^T \dot{\xi}_i^{ref}}{\|f(\xi_i^{ref})\| \|\dot{\xi}_i^{ref}\|}|$

(iii) dynamic time warping distance as in [26]. RMSE and  $\hat{e}$  provide an overall assessment of the similarity between the resulting DS and the demonstration, and DTWD measures the dissimilarity between the reference trajectory and the corresponding reproduction from the same starting points.

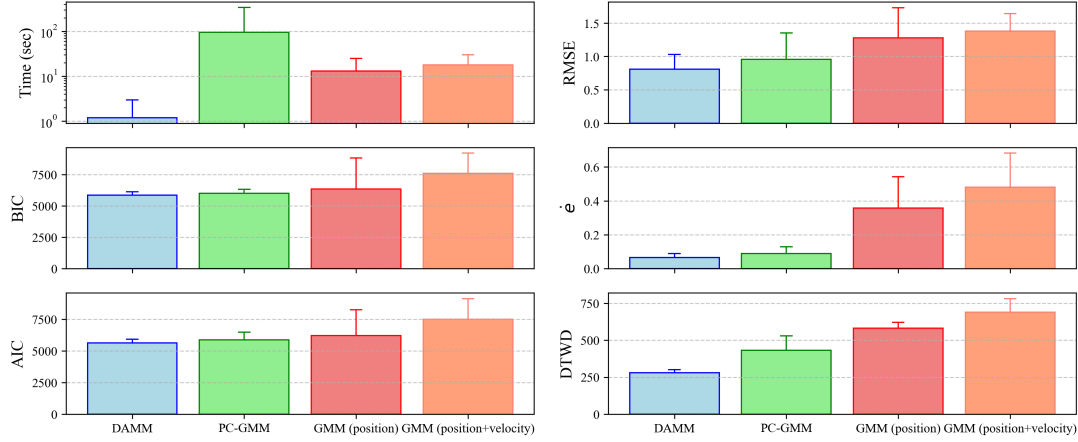


Fig. 2: Comparison of the average performance between DAMM and PC-GMM over the entire LASA dataset, with the bar and whisker depicting the mean and standard deviation respectively. Notice the drastic decrease in computation time (top left plot) of DAMM vs. PC-GMM.

Fig. 2 compares the performance between DAMM, PC-GMM and two baseline GMM methods across all 6 metrics. Notably, the computation time on the upper left shows that DAMM exhibits significant speedup. We show that the DAMM-based LPV-DS method can efficiently learn a task involving 700 observations in just about 1 second, while the PC-GMM method requires 50 seconds. The distinction becomes even more pronounced when dealing with larger datasets. For example, given a demonstration of 7000 observations, DAMM completes the clustering of the trajectory within 5 seconds, whereas PC-GMM takes more than 1 hour due to its incremental nature. It’s notable that the computation time of PC-GMM grows exponentially with the size of observations, while DAMM exhibits linear growth.

We observe that the other two metrics, BIC and AIC (lower the better) in the left column of Fig. 2, show that DAMM holds a slight advantage over the PC-GMM in achieving an efficient and accurate model without compromising model complexity. Note that while the margin of difference between two models is not statistically significant, DAMM remains comparable to the state-of-the-art level of model efficiency. In the right column of Fig. 2, DAMM shows a small edge over PC-GMM in DS performance over the three metrics (lower the better). The non-significant difference is unsurprising, given that both models effectively capture trajectory direction and generate appropriate models, leading to proper DS through proceeding optimization.

We provide visualization of the DAMM clustering results and corresponding LPV-DS vector flows for the LASA dataset in Appendix G. Further, we provide visualization of clustering and LPV-DS results on the dataset provided by the accompanying code of the PC-GMM approach in Appendix H. Further, in Appendix E we provide a computation time comparison of DAMM on different cores compared to PC-GMM for a large dataset, as shown PC-GMM takes 20min to fit a GMM, whereas DAMM finishes in 10s with 4 cores.

We conclude that DAMM significantly outperforms its predecessor in computational speed, while maintaining model efficiency and DS quality on par with the current state of the art.

### 3.2. Robot Experiments

We validate DAMM on a Frank Emika robot by learning DS-based motion policies from demonstrations. Fig. 3 shows an example of learning a multi-modal demonstration. The upper row shows that DAMM produces suitable clustering results, and the resulting DS reproduces the original demonstration while generalizing to other unexplored regions. Franka then executes the learned DS as its motion policy, showing that its end-effector follows the learned trajectory and reaches the attractor from different initial positions. In addition, by adding perturbations to the robot along the motion, the robot adjusts itself and reaches the attractor with stability. We further show an application of DAMM in an incremental learning context in Appendix F.



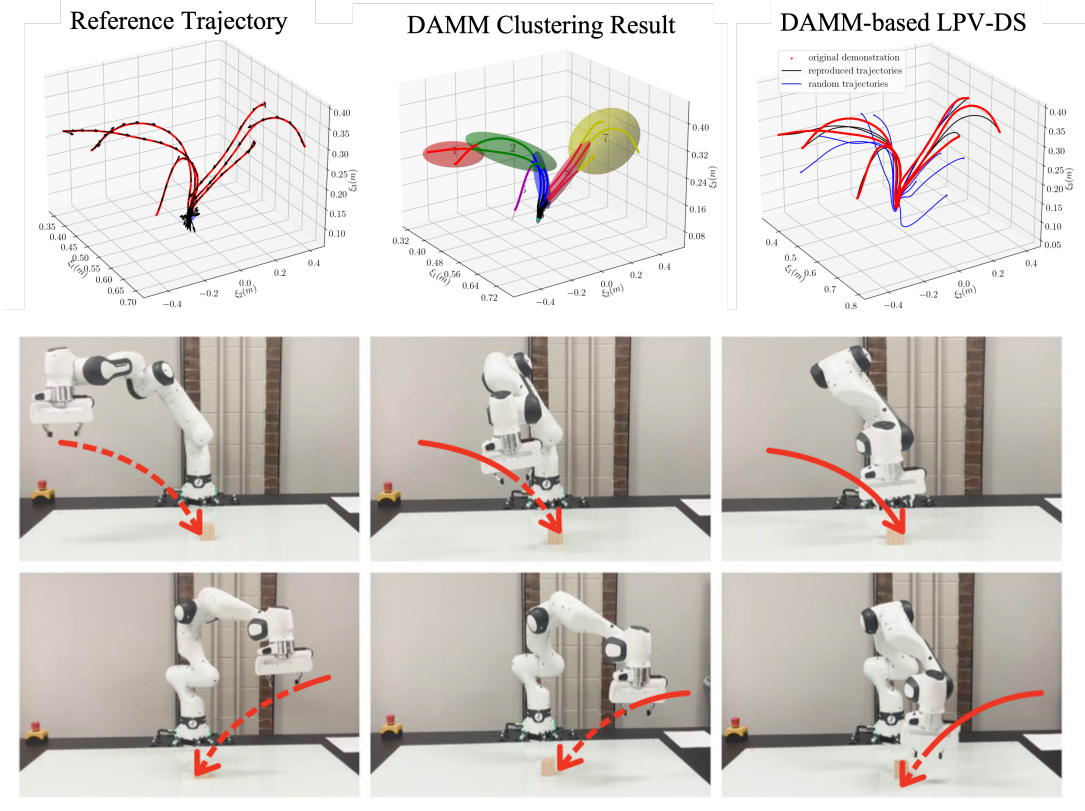


Fig. 3: Learning a multi-model demonstration in DAMM-based LPV-DS framework.

#### 4. Conclusion and Limitation

In this paper, we introduce the Directionality-aware Mixture Model that is capable of effectively identifying the directional features of the trajectory data. By taking into account both the positional and directional information, DAMM can produce physically-meaningful clustering results that represent the intrinsic structure of the trajectory data. Along with the parallel sampling scheme, the new DAMM-based LPV-DS framework achieves significant improvement in computational efficiency while remaining comparable to the state-of-the-art level of model efficiency.

##### Limitation

In many scenarios, even the directional features may fail to convey enough information about the trajectory data or even lead to erroneous clustering results. Imagine a self-intersecting trajectory, for example, a circle, the trajectory will enter and leave the circle at the same position and in the same direction. It will lead to DAMM erroneously clustering both the entry and exit portions as one component because they are close in both positional and directional sense. To distinguish between trajectories with the same directionality, it may become necessary to include even sequential information to introduce another dimension for future work.

## References

- [1] A. Ude. Trajectory generation from noisy positions of object features for teaching robot paths. *Robotics and Autonomous Systems*, 11(2):113–127, 1993. ISSN 0921-8890. doi: [https://doi.org/10.1016/0921-8890\(93\)90015-5](https://doi.org/10.1016/0921-8890(93)90015-5).
- [2] J.-H. Hwang, R. Arkin, and D.-S. Kwon. Mobile robots at your fingertip: Bezier curve on-line trajectory generation for supervisory control. volume 2, pages 1444 – 1449 vol.2, 11 2003. ISBN 0-7803-7860-1. doi: 10.1109/IROS.2003.1248847.
- [3] J. Aleotti and S. Caselli. Robust trajectory learning and approximation for robot programming by demonstration. *Robotics and Autonomous Systems*, 54(5):409–413, 2006. ISSN 0921-8890. doi: <https://doi.org/10.1016/j.robot.2006.01.003>.
- [4] S. M. Khansari-Zadeh and A. Billard. Imitation learning of globally stable non-linear point-to-point robot motions using nonlinear programming. In *2010 IEEE/RSJ International Conference on Intelligent Robots and Systems*, pages 2676–2683, 2010. doi: 10.1109/IROS.2010.5651259.
- [5] E. Gribovskaya, S.-M. Khansari-Zadeh, and A. Billard. Learning non-linear multivariate dynamics of motion in robotic manipulators. *The International Journal of Robotics Research*, 30(1):80–117, 2011. doi: 10.1177/0278364910376251.
- [6] S. M. Khansari-Zadeh and A. Billard. Learning stable non-linear dynamical systems with gaussian mixture models. *IEEE Transactions on Robotics*, 27(5):943–957, 2011.
- [7] N. Figueroa and A. Billard. A physically-consistent bayesian non-parametric mixture model for dynamical system learning. In *Proceedings of The 2nd Conference on Robot Learning*, volume 87, pages 927–948. PMLR, 2018.
- [8] A. Billard, S. Mirrazavi, and N. Figueroa. *Learning for Adaptive and Reactive Robot Control: A Dynamical Systems Approach*. The MIT Press, 2022. ISBN 9780262046169.
- [9] H. K. Khalil. *Nonlinear systems; 3rd ed*. Prentice-Hall, Upper Saddle River, NJ, 2002. URL <https://cds.cern.ch/record/1173048>. The book can be consulted by contacting: PH-AID: Wallet, Lionel.
- [10] D. Blei and P. Frazier. Distance dependent chinese restaurant processes. *Journal of Machine Learning Research*, 12: 2461–2488, 08 2011.
- [11] J. Straub, J. Chang, O. Freifeld, and J. Fisher III. A Dirichlet Process Mixture Model for Spherical Data. In *Proceedings of the Eighteenth International Conference on Artificial Intelligence and Statistics*, volume 38 of *Proceedings of Machine Learning Research*, pages 930–938. PMLR, 09–12 May 2015.
- [12] S. M. Khansari-Zadeh and A. Billard. Learning control lyapunov function to ensure stability of dynamical system-based robot reaching motions. *Robotics and Autonomous Systems*, 62(6):752–765, 2014.
- [13] M. do Carmo. *Riemannian Geometry*. Mathematics (Boston, Mass.). Birkhäuser, 1992. ISBN 9783764334901.
- [14] J. Lee. *Introduction to Riemannian Manifolds*. Graduate Texts in Mathematics. Springer International Publishing, 2019. ISBN 9783319917542.
- [15] M. Arnaudon, F. Barbaresco, and L. Yang. Medians and means in riemannian geometry: Existence, uniqueness and computation. 11 2011. doi: 10.1007/978-3-642-30232-9.8.
- [16] X. Pennec. Intrinsic statistics on riemannian manifolds: Basic tools for geometric measurements. *Journal of Mathematical Imaging and Vision*, 25:127–154, 07 2006. doi: 10.1007/s10851-006-6228-4.
- [17] M. J. A. Zeestraten, I. Havoutis, J. Silvério, S. Calinon, and D. G. Caldwell. An approach for imitation learning on riemannian manifolds. *IEEE Robotics and Automation Letters*, 2(3):1240–1247, 2017. doi: 10.1109/LRA.2017.2657001.
- [18] S. Calinon. Gaussians on riemannian manifolds: Applications for robot learning and adaptive control. *IEEE Robotics & Automation Magazine*, 27(2):33–45, 2020. doi: 10.1109/MRA.2020.2980548.
- [19] J. Sethuraman. A constructive definition of dirichlet priors. *Statistica Sinica*, 4(2):639–650, 1994. ISSN 10170405, 19968507.
- [20] K. P. Murphy. Conjugate bayesian analysis of the Gaussian distribution. 2007.
- [21] R. M. Neal. Markov chain sampling methods for dirichlet process mixture models. *Journal of Computational and Graphical Statistics*, 9(2):249–265, 2000.
- [22] J. Chang and J. W. Fisher III. Parallel sampling of DP mixture models using sub-cluster splits. In *Advances in Neural Information Processing Systems*, volume 26, 2013.
- [23] S. Jain and R. M. Neal. A split-merge markov chain monte carlo procedure for the dirichlet process mixture model. *Journal of Computational and Graphical Statistics*, 13(1):158–182, 2004. doi: 10.1198/1061860043010.
- [24] N. Metropolis, A. W. Rosenbluth, M. N. Rosenbluth, A. H. Teller, and E. Teller. Equation of state calculations by fast computing machines. 3 1953. doi: 10.2172/4390578.
- [25] W. K. Hastings. Monte carlo sampling methods using markov chains and their applications. *Biometrika*, 57(1):97–109, 1970. ISSN 00063444.
- [26] J. R. Medina and A. Billard. Learning stable task sequences from demonstration with linear parameter varying systems and hidden markov models. In *Proceedings of the 1st Annual Conference on Robot Learning*, volume 78 of *Proceedings of Machine Learning Research*, pages 175–184. PMLR, 13–15 Nov 2017.

## Appendix

### A. Proof of LPV-DS Stability

A dynamical system  $\dot{\xi} = f(\xi)$ ,  $\xi \in \mathbb{R}^d$  is said to be asymptotically stable if there exists a Lyapunov function  $V : \mathbb{R}^d \rightarrow \mathbb{R}$  such that:

1.  $V(\xi)$  is continuously differentiable.
2.  $V(\xi)$  is positive definite, i.e.,  $V(\xi) > 0$  for all  $\xi \neq 0$ , and  $V(0) = 0$ .
3.  $\dot{V}(\xi) = \frac{dV}{dt} = \nabla V(\xi) \cdot f(\xi)$  is negative definite, i.e.,  $\dot{V}(\xi) < 0$  for all  $\xi \neq 0$ .

In our quadratic Lyapunov function formulation  $V(\xi) = (\xi - \xi^*)^T P (\xi - \xi^*)$ , the function satisfies the first two Lyapunov conditions because it is continuously differentiable, and by designating  $P$  as a symmetric positive definite matrix, we ensure that  $V(x)$  is positive definite. Furthermore,  $V(x) = 0$  only when  $\xi = \xi^*$ .

To prove the third condition, firstly we take derivative of  $V(\xi)$  w.r.t time  $t$ :

$$V(\dot{\xi}) = (\xi - \xi^*)^T P f(\xi) + f(\xi)^T P (\xi - \xi^*) \quad (13)$$

Plug  $f(\xi) = \sum_{k=1}^K \gamma_k(\xi)(A_k \xi + b_k)$  into Eq. 13:

$$V(\dot{\xi}) = (\xi - \xi^*)^T P \sum_{k=1}^K \gamma_k(\xi)(A_k \xi + b_k) + \sum_{k=1}^K \gamma_k(\xi)(A_k \xi + b_k)^T P (\xi - \xi^*) \quad (14)$$

Then substitute  $b_k$  with  $-A_k \xi^*$  according to Eq. 19:

$$V(\dot{\xi}) = (\xi - \xi^*)^T P \sum_{k=1}^K \gamma_k(\xi)(A_k \xi - A_k \xi^*) + \sum_{k=1}^K \gamma_k(\xi)(A_k \xi - A_k \xi^*)^T P (\xi - \xi^*) \quad (15)$$

Finally:

$$V(\dot{\xi}) = (\xi - \xi^*)^T P \left( \sum_{k=1}^K \gamma_k(\xi) A_k \right) (\xi - \xi^*) + (\xi - \xi^*)^T \left( \sum_{k=1}^K \gamma_k(\xi) A_k^T \right) P (\xi - \xi^*) \quad (16)$$

$$= (\xi - \xi^*)^T \left( \left( \sum_{k=1}^K \gamma_k(\xi) (P A_k + (A_k)^T P) \right) (\xi - \xi^*) \right) \quad (17)$$

According to Eq. 19, we should ensure that  $A_k^T P + P A_k \prec Q_k \prec 0$ ,  $\forall k = 1 \dots K$  and  $\gamma_k(\xi) > 0$ , therefore  $V(\dot{\xi})$  always being less than 0 except when  $\xi = \xi^*$ . Thus, any learned dynamical systems with constraints specified in Eq. 1 will be globally asymptotically stable.

### B. Details of Optimization Formulation

As mentioned in the LPV-DS formulation section, we represent the nonlinear Dynamic System (DS) as a combination of continuous, time-invariant linear systems:

$$\dot{\xi} = f(\xi) = \sum_{k=1}^K \gamma_k(\xi)(A_k \xi + b_k), \quad (18)$$

$\gamma_k(x)$  quantifies the weight of each linear system, ensuring the smoothness of the reproduced trajectories. We then estimate the parameters of each subsystem  $\Theta = \{A_k, b_k\}_{k=1}^K$ . To maintain both the precision of the reproduction and the stability of the system, we adopt the formulation in [7] and construct a semi-definite optimization problem by minimizing the velocity error between the reference and prediction,

$$\begin{aligned} & \underset{\theta_f}{\text{minimize}} && \sum_{n=1}^{N_{\text{ref}}} \sum_{t=1}^{T_N} \left\| \dot{\xi}_{t,n}^{\text{ref}} - f(\xi_{t,n}^{\text{ref}}) \right\|^2 \\ & \text{subject to} && A_k^T P + P A_k \prec Q_k, \quad \forall k = 1, \dots, K, \\ & && Q_k = Q_k^T \prec 0, \\ & && b_k = -A_k \xi^* \end{aligned} \quad (19)$$

where  $N_{ref}$  is the number of trajectories from the demonstration,  $T_N$  is the total amount of recorded states in each trajectory,  $t$  is the sequence order of sampled states in the corresponding demonstration trajectory, and  $\xi^*$  is the common attractor for all demonstration trajectories.

The parameters  $Q_k$  enable a larger search space for parameters. Under the quadratic Lyapunov function  $V(\xi) = (\xi - \xi^*)^T P (\xi - \xi^*)$ , this formulation ensures the convergence and stability of the system.

### C. Unit Sphere Manifold

Given  $x, y \in \mathbb{S}^d$ , the exponential and logarithmic maps are defined as:

$$y = \exp_x(u) = x \cos(\|u\|) + \frac{u}{\|u\|} \sin(\|u\|), \quad (20)$$

$$u = \log_x(y) = d(x, y) \frac{y - x^T y x}{\|y - x^T y x\|} \quad (21)$$

where the geodesic distance is  $d(x, y) = \arccos(x^T y)$ . Note that in the above representation,  $u$  and  $v$  are the vectors mapped in  $T_x \mathbb{S}^d$ .

### D. Merge Proposal Formulation

Eq. 10 shows that for either a split or merge proposal, one need to evaluate the ratio of target distribution and proposal distribution. Similar to split proposal splitting one group into two, merge proposal in the inverse operation that attempts to merge two existing components into one. This is done by first performing intermediate IW Gibbs sampler to reach the launch state  $z^{launch}$  and then evaluate the following expressions:

$$\frac{p(z^{merge}|\xi)}{p(z|\xi)} = \frac{\prod_{z_i=z_{12}^{merge}} \mathcal{N}(\xi_{z_i}|\mu, \Sigma)_{\{z_{12}^{merge}\}}}{\prod_{z_i=z_1^{merge}} \pi_1 \mathcal{N}(\xi_{z_i}|\mu, \Sigma)_{\{z_1^{merge}\}} \prod_{z_i=z_2^{merge}} \pi_2 \mathcal{N}(\xi_{z_i}|\mu, \Sigma)_{\{z_2^{merge}\}}} \quad (22)$$

$$\frac{P(z|z^{merge})}{P(z^{merge}|z)} = \prod_{z_i=z_1^{launch}} \prod_{z_i=z_2^{launch}} \frac{\pi_{z_i} \mathcal{N}(\xi_{z_i}|\mu, \Sigma)_{\{z_i\}}}{\pi_{z_1^{launch}} \mathcal{N}(\xi_{z_i}|\mu, \Sigma)_{\{z_1^{launch}\}} + \pi_{z_2^{launch}} \mathcal{N}(\xi_{z_i}|\mu, \Sigma)_{\{z_2^{launch}\}}} \quad (23)$$

where  $\{z_1^{merge}\}$  is the first group of observations before merging,  $\{z_2^{merge}\}$  is the second group of observations before merging,  $\{z_{12}^{merge}\}$  is the combined group of observations after merging. When a merge proposed, one can evaluate each expression in Eq. 22 and Eq. 23 and plug the value back to the Eq. 10 to evaluate if the merge is accepted or not.

### E. Further DAMM vs. PC-GMM Computation Time Evaluation

Figure 4 shows the computation time on a large dataset of 3500 points, highlighting that PC-GMM requires over 20 minutes to complete the clustering, whereas DAMM, utilizing the maximum number of available threads, finishes in 10 seconds.

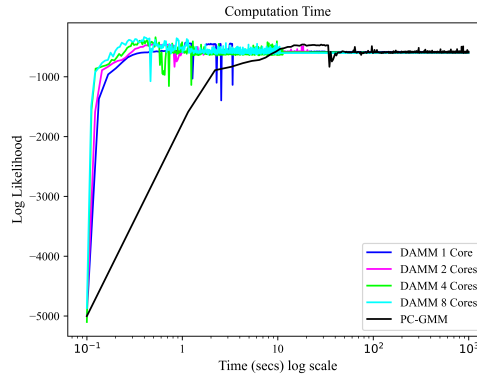


Fig. 4: Log likelihood versus time between DAMM performed on different numbers of cores and PC-GMM on LASA Multi\_Models\_4 dataset

## F. Incremental Learning

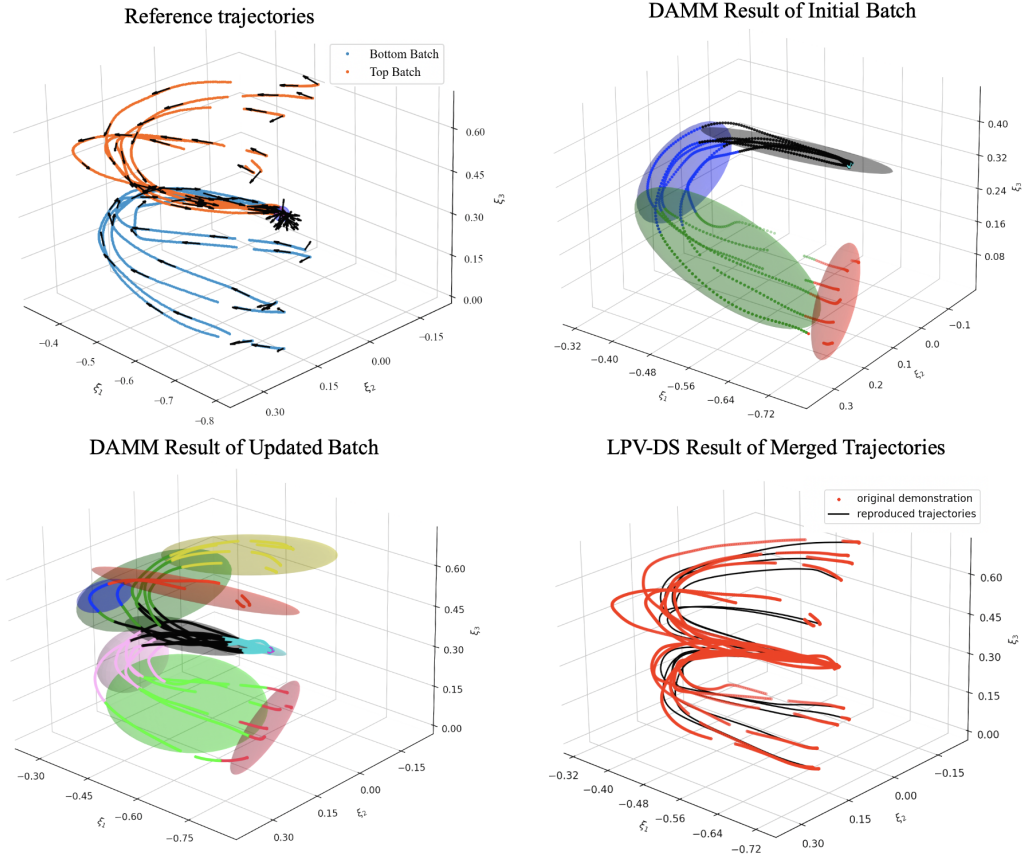


Fig. 5: DAMM-based LPV-DS incremental learning of a shelf-arranging demonstration

Another notable advantage of DAMM is its capability for incremental learning, which would otherwise be costly for other methods. In scenarios where multiple batches of data need to be learned incrementally, the previous LPV-DS framework would require re-learning the entire batch, resulting in significant computational inefficiency. In Figure 5, we show that DAMM can incrementally learn two batches of shelf-arranging demonstrations obtained from the accompanying code of PC-GMM [7]. To DAMM, an incoming new batch is considered as a new component, and the sampling method will determine if a split or merge *w.r.t.* of the existing components is appropriate or not.



## G. LASA Dataset Benchmark

Every three rows show the results of five different datasets, with the first row showing the clustering results of DAMM, the second showing the probability density function of the mixture model, and the last row showing the generated DS.

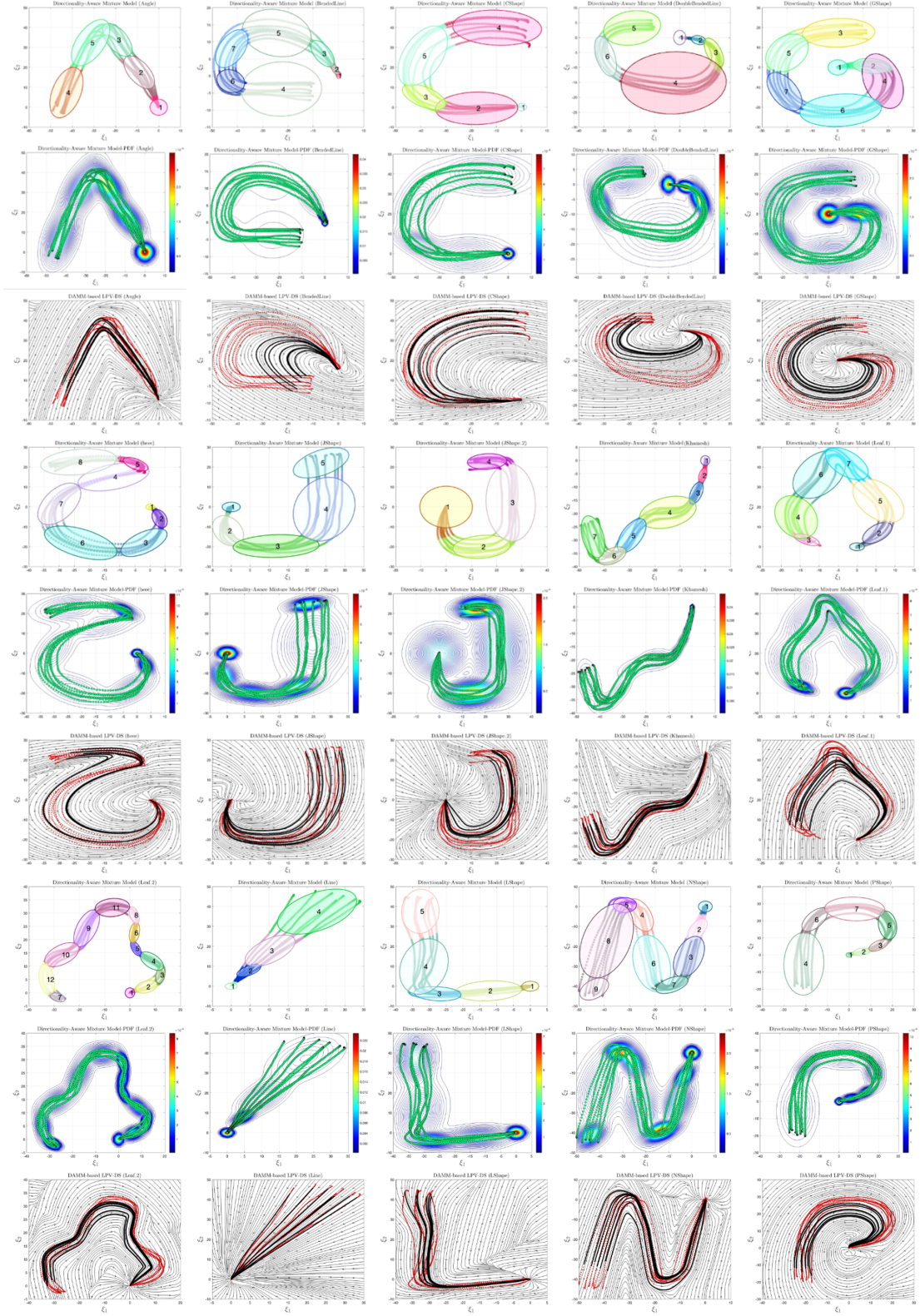


Fig. 6: Results on the LASA Dataset with Learned Clusters and Reproduced Stream Graph using DAMM (Part 1).

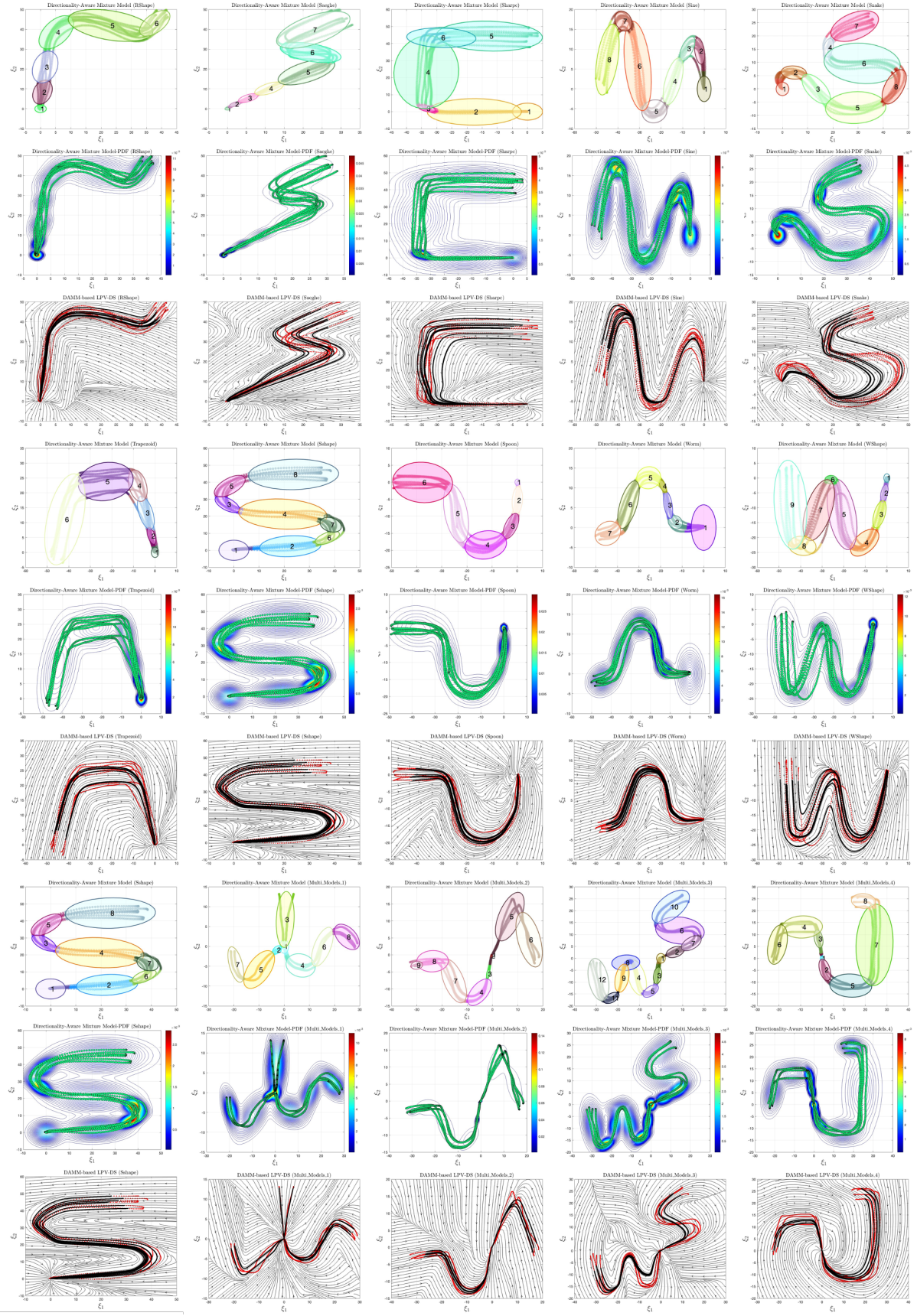
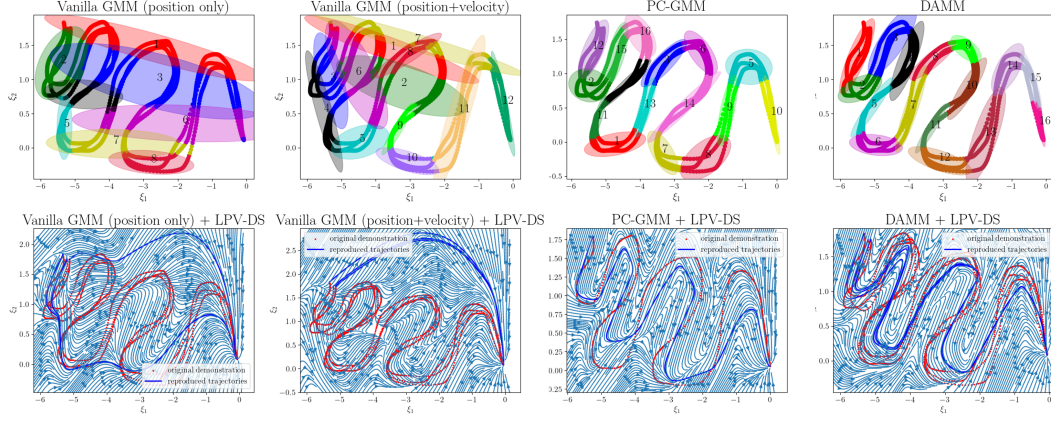


Fig. 7: Results on the LASA Dataset with Learned Clusters and Reproduced Stream Graph using DAMM (Part 2)

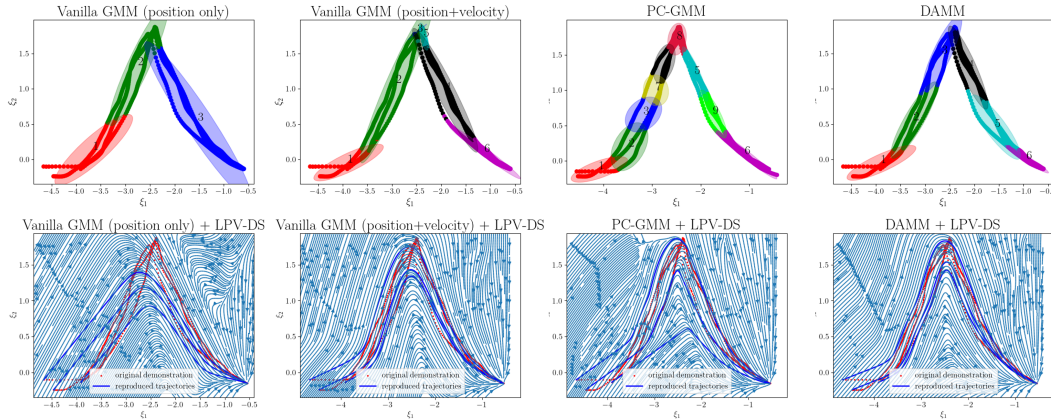


## H. PC-GMM [7] Dataset Benchmark

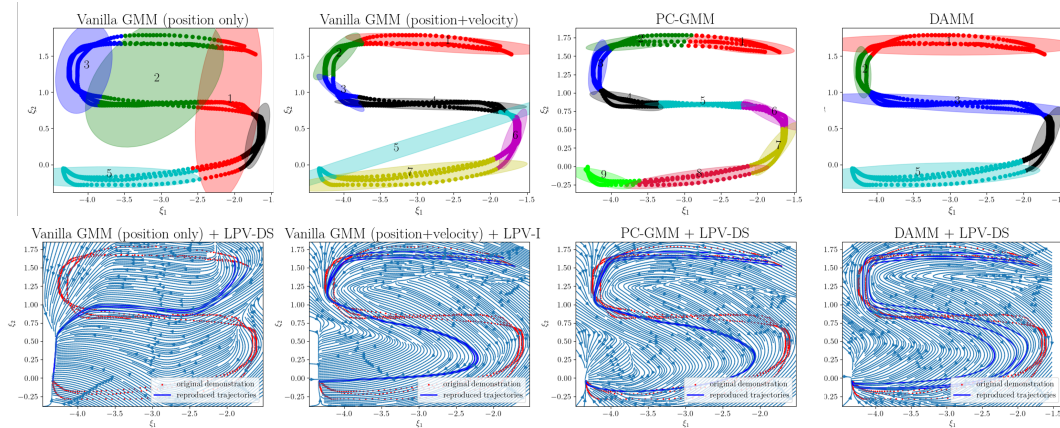
Comparison between the Vanilla-GMM (position only) LPV-DS, Vanilla-GMM (position+velocity) LPV-DS, PC-GMM LPV-DS and **DAMM LPV-DS** on the PC-GMM benchmark dataset (2D and 3D real trajectories) [7]. We show the number of components and computation of each method from left to right. Notice the improved reproduction accuracy resulting from optimal GMM fitting via DAMM on the right column.



Number of components: 8, 12, 16, 16. Computation time in seconds: 5, 6, 58, 1

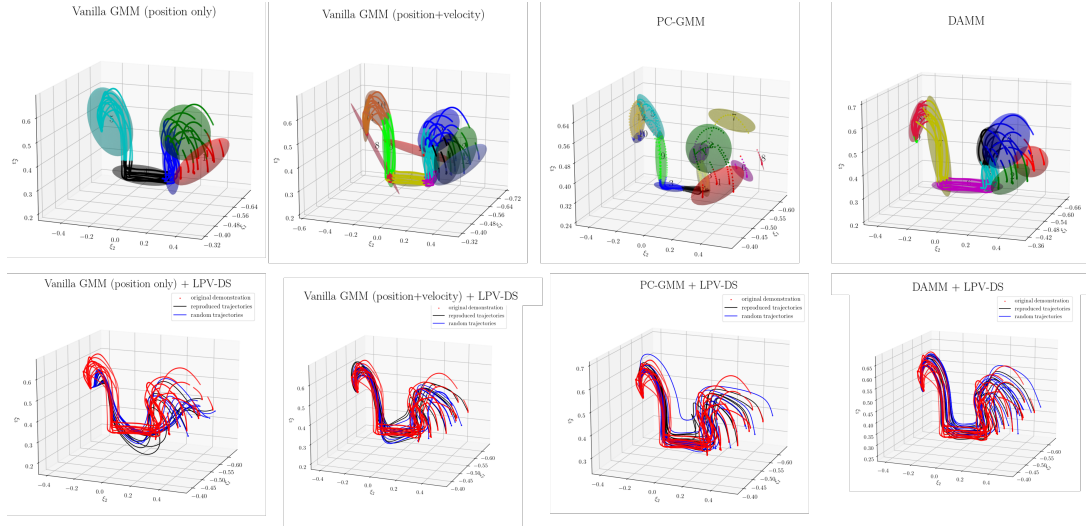


Number of components: 3, 6, 9, 6. Computation time in seconds: 3, 4, 47, 0.5

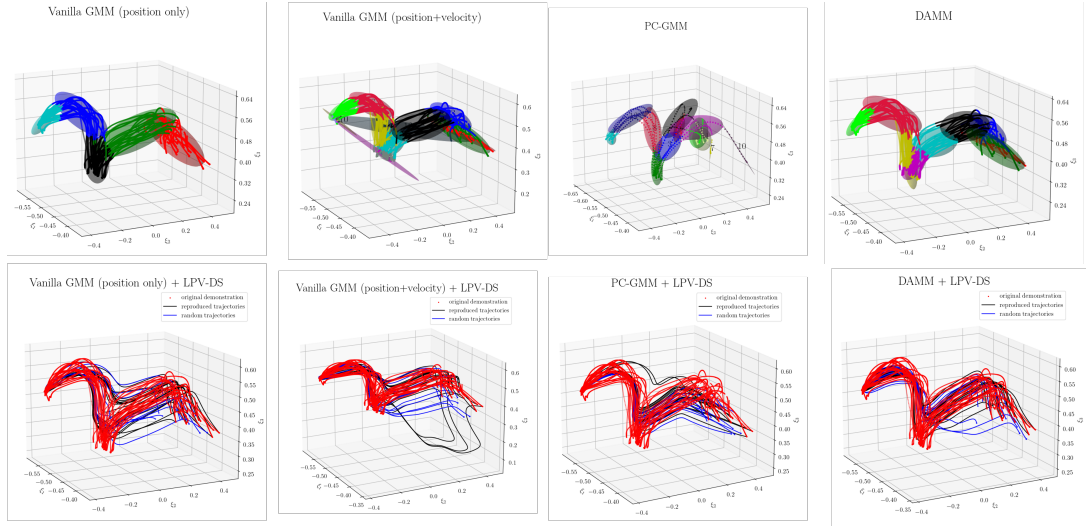


Number of components: 5, 7, 9, 5. Computation time in seconds: 3, 5, 60, 0.7

Fig. 8: 2D real trajectories ( $< 1000$  observations) from PC-GMM benchmark dataset: messy snake shape, A shape and S shape from top to bottom



Number of components: 5, 10, 12, 9. computation time in seconds: 8, 10, 3700, 1.7



Number of components: 5, 11, 12, 9. computation time in seconds: 6, 8, 4200, 1.4

Fig. 9: 3D real trajectories from PC-GMM benchmark dataset: sink shape (4671 observations) and via shape (3786 observations) from top to bottom. Notice the PC-GMM took exponentially longer time in large dataset